Remarkable Enhancement of Catalytic Activity of Cu-Complexes in the Electrochemical Hydrogen Evolution Reaction (HER) by Using Triply-Fused Porphyrin

Shubhadeep Chandra,[†,#] Arijit Singha Hazari,[†,#] Qian Song,[§] David Hunger,[‡] Nicolás I. Neuman,[†] Joris van Slageren,*[,‡] Elias Klemm,*[,§] Biprajit Sarkar*[,†]

[†]Lehrstuhl für Anorganische Koordinationschemie, Institut für Anorganische Chemie, Universität Stuttgart, Pfaffenwaldring 55, D-70569, Stuttgart, Germany, Email: biprajit.sarkar@iac.uni-stuttgart.de

Instituto de Desarrollo Tecnológico para la Industria Química, INTEC, UNL-CONICET, Predio CONICET Santa Fe Dr. Alberto Cassano, Ruta Nacional N° 168, Km 0, Paraje El Pozo, (S3000ZAA) Santa Fe, Argentina.

[‡]Institut für Physikalische Chemie, Universität Stuttgart, 70569 Stuttgart, Germany

[§]Institute of Chemical Technology, University of Stuttgart, Pfaffenwaldring 55, 70569, Stuttgart, Germany

[#]S.C and A.S.H contributed equally

Abstract:

Developing efficient molecular catalysts for the electrocatalytic hydrogen evolution reaction (HER) is a highly important goal in contemporary science. We report here on a bimetallic triply fused copper porphyrin complex (**1**) comprising two monomeric porphyrin units linked through β–β, *meso–meso*, β′–β′ triple covalent linkages, that exhibits remarkable enhancement of catalytic activity for the electrochemical HER in comparison to the analogous monomeric copper porphyrin complex (**2**). Spectroscopic characterization, in association with magnetic measurements, clearly establish the ground state structures of both the bimetallic and monometallic complexes as containing two and one copper (II) centers, respectively. The fused metalloporphyrin complex is found to undergo electrochemical reduction at a lower negative applied potential compared to the metalloporphyrin monomer, as evident from the significant anodic shift (~800mV) in the potential of the first reduction process. Electrochemical investigations in the presence of a proton source (trifluoroacetic acid) confirm that the catalytic activity of the fused metalloporphyrin occurs at a significantly lower onset potential, (overpotential decreased by ~320 mV), compared to the non-fused monomer. Controlled potential electrolysis combined with the kinetic analysis of catalysts **1** and **2** confirm the production of hydrogen, with 96% and 71% faradaic efficiencies and turnover numbers of 102 and 18, respectively. Kinetic investigations further reveal an observed rate constant of around 10^7 (s^{-1}), implying high efficiency of the bimetallic catalyst towards hydrogen evolution reaction. Mechanistic insights are presented by using a combination of UV-vis-NIR and EPR spectroscopy and electrochemistry. Our results thus firmly establish the triply fused porphyrin ligands as candidates for generating highly efficient molecular electrocatalysts in combination with transition metal centers.

Introduction:

Limited resources of non-renewable energy, rapid depletion of fossil fuels, and ever-increasing energy demands have led to a global search for alternative energy sources.[1] Hydrogen as an energy carrier is considered as one of the promising alternatives to conventional energy sources as it is carbon free and, upon combustion, generates environmentally benign by-product H_2O, resulting in a carbon neutral energy production system.[2,3] Electrocatalytic reduction of protons utilizing renewable energy sources is one of the most promising strategies for converting electrical energy to chemical energy through sustainable production of hydrogen.[4] Electrocatalytic hydrogen evolution reaction (HER) ($2H^+ + e^- \rightarrow H_2$), fundamental to various energy transfer related chemical transformations, has garnered considerable attention as a new paradigm for energy storage, delivery and transport.[5] Elemental platinum is the long established industrial catalyst for electrocatalytic production of hydrogen; however, low natural abundance and high cost of this noble metal limits large-scale applications in H_2 production, prompting researchers to seek alternative non-noble metal-based catalysts.[3] In the past decade, substantial effort and time have been devoted towards finding cheap, efficient and robust catalysts comprised of earth-abundant elements for HER.[6,7] As a result, several transition metal complexes of earth-abundant elements like Fe,[8] Co,[9] Mo,[10] Cu[11] and Ni[12] have been recognized as active molecular electrocatalysts for HER. In addition to homogeneous systems, molecular catalysts immobilized on carbon nanotube-templated covalent frameworks, have also been identified as active catalysts for the proton reduction reaction in aqueous medium.[13] Although solid state supported catalysts find extensive application in various technological processes, due to recyclability and easy separation of the catalyst, homogeneous catalysis provides greater control over physical properties as evident from the well-defined active sites of the catalysts. Besides, investigation of homogeneous catalytic processes divulges significant insight into the mechanistic pathways, thus providing plausible explanations behind structure-activity relationships governing catalytic activity. [14,15]

In natural environments, hydrogenase enzymes containing [Fe-Fe] or [Fe-Ni] active sites catalyse reversible interconversion of protons into hydrogen with a low overpotential and turnover frequency as high as 10000 s^{-1}, which highlights the importance of noble metal free bimetallic catalysts.[16] However, challenges related to isolation and utilization of these enzymes under non-natural environments have prompted researchers to seek structural and functional models mimicking the active site of hydrogenase.[17] Considerable efforts for designing robust catalytic systems capable of matching the efficiency of enzymatic systems resulted in various inorganic model complexes that have provided mechanistic insight into the

functioning of enzymes. However, high overpotential, low turnover number, low rate constants, easy catalyst decomposition under electrocatalytic conditions and requirement of strong acids often prohibit their widespread applications in catalytic systems.[15] Moreover, several functional analogues based on bimetallic electrocatalysts inspired by natural enzymes have been designed and in some cases they exhibit superior catalytic efficiency as compared to their monomeric counterparts.[18]

In this context, transition metal complexes of tetrapyrrolic macrocycles such as porphyrin are important due to their unique physicochemical properties and unprecedented reactivity of the metalloporphyrin frameworks.[19] From the perspective of electrocatalysis, metalloporphyrins have been shown to efficiently catalyze the reduction of protons into hydrogen as well as reduction of CO_2 into different C1 products.[20] On this ground, several Fe, Ni, Co and Cu complexes of porphyrins have gained significant attention as HER catalysts.[21] The advantage of porphyrinic frameworks over other molecular catalysts lies in the ease with which the substitution pattern at the periphery controls proton transfer ability, substrate accessibility and selectivity in product formation.[22,23] The influence of hanging carboxylic groups at the backbone of Ni(II) hangman porphyrins, towards HER activity mediated by proton coupled electron transfer activity has been demonstrated.[22] Although a wide range of earth abundant elements have been identified as potential electrocatalyst for HER, there is a dearth of reports involving Cu-based electrocatalytic systems for the proton reduction reaction, which is quite surprising considering several documented examples highlighting the role of Cu-based catalysts in CO_2 or water oxidation reactions.[7,24] Recent works from Cao and co-workers, as well as from Gross and co-workers are among the handful of examples showing the role of Cu-corroles in electrocatalytic HER.[25] One of the possible reasons is that copper-based molecular catalysts have an enhanced propensity to undergo demetallation under reducing conditions, forming Cu-nanoparticles or depositing on electrodes, all of which can catalyze HER in their own right. Thus, the contemporary challenges in developing molecular electrocatalysts are to find systems that will function at low over-potentials, deliver high turnover numbers and rate constants, and be robust towards decomposition under electrocatalytic conditions, particularly while generating high current densities. The latter point remains an often unaddressed question in molecular electrocatalysis.

Whereas, metal complexes of monoporphyrin have been exploited extensively for electrocatalytic HER, OER and CO_2 reduction reactions, similar studies comprising fused porphyrins have been reported only once (see below). Fused porphyrins are unique structural motifs, where two monoporphyrin units are connected via β–β, *meso–meso*, β′–β′ triple covalent

linkages.[26] Electrocatalytic properties of metal complexes of fused porphyrins could be intriguing due to favourable properties including ability to undergo reduction or oxidation at lower applied potentials compared to their monomeric counterparts and extensive delocalization of electrons across the conjugated frameworks. Fused porphyrins also provide an alternative to the peripheral perturbation imparted by the change in electronic nature of the functional groups. In this context, Moore and co-workers for the very first time illustrated enhanced catalytic efficiency of doubly fused bimetallic copper porphyrins over the analogous nonfused monomeric copper porphyrin, in electrocatalytic HER.[27] A recent study by Apfel and co-workers further exemplified the superior catalytic efficiency of a bimetallic macrocycle featuring two cofacially linked Ni(II)-porphyrin by a linker molecule.[28]

In the present contribution, we report the first example of HER catalysts based on the triply-fused bimetallic copper porphyrin (**1**) and draw a comparison of the fused complex's catalytic activity with that of the analogous monomeric Cu-porphyrin (**2**) and bimetallic zinc porphyrin (**3**) (Chart I).

Chart-I: Molecular Structures of the Complexes Studied in this Work
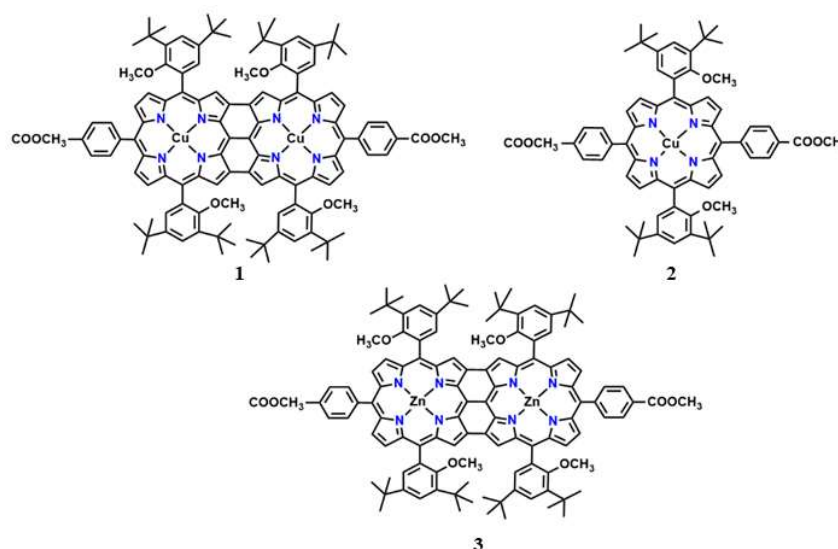
Both complexes were synthesized and characterized by a combination of various experimental techniques including cyclic voltammetry, EPR/UV-Vis-NIR spectroelectrochemistry and density functional theory calculations. Electrochemical techniques are utilized to investigate the catalytic activity of both the fused and monoporphyrin complexes towards proton reduction in non-aqueous media in the presence of TFA as a proton source. Different kinetic and thermodynamic factors governing the catalytic activity of the complexes were extracted from various electrochemical experiments. The main aim of this work is the development of an electrocatalytic system for the HER that will allow the generation of high current densities while operating at low overpotentials, and still deliver high turnover numbers and rate constants. To

the best of our knowledge, this is the first report on the electrocatalytic activity of a metal complex with a triply fused porphyrin ligand, and the system presented here fullfill all the aforementioned sought after parameters for molecular electrocatalysts.

## Results and Discussion

Synthesis and Electrochemistry

Dinuclear and mononuclear copper complexes **1** and **2** were synthesized by insertion of copper into the free-base fused dimeric porphyrin and its tetrasubstituted monomeric analogue by the reaction of copper acetate with free base porphyrin in a chloroform/methanol (10:1) solvent mixture, at room temperature (**2**) and under refluxing condition (**1**). Purification of the crude material via column chromatography and recrystallization from chloroform/methanol yielded violet-colored pure compound in moderate yields. Characterization of all the precursor materials (complexes **3**, **5**, **6**, **7**) and the fused and monomeric porphyrin complexes (**1** and **2**) have been carried out utilizing a combination of experimental techniques such as ESI-MS, ^{1}H-NMR, UV-Vis-NIR absorption and EPR spectroscopy to ascertain the molecular identity of the target compounds (Figures S1-S6, Experimental details, Supporting Information). The triply fused bimetallic porphyrin exhibited characteristic NMR signals, as reported in the literature, [26b] in which peaks are shifted to higher fields attributed to the effect of π-electron delocalization on the ring current of the array. Crystals suitable for X-Ray diffraction were obtained via slow diffusion of a benzene solution of the complex into ethanol; however, due to the poor quality of the crystal data, bond parameters have not been discussed, although the core structure of the ligand along with the coordination mode of the metal is unequivocally established. From the molecular structure, a planar conformation of the fused ligand scaffold is observed, where two copper centers coordinate to four tetrapyrrolic nitrogen atoms of the individual porphyrin units, indicating coplanar arrangements of the copper and ligand framework (Figure S7, Supporting Information).

Electrochemical properties of the synthesized complexes have been evaluated via cyclic voltammetric (CV) and differential pulse voltammetric (DPV) analysis in *N,N,*-dimethylformamide (DMF) containing 0.1 M tetrabutylammonium hexafluorophosphate (^{n}Bu$_4$PF$_6$) as the supporting electrolyte, at 100 mV/s scan rate. Cyclic voltammograms of the dinuclear complex **1** display multiple redox processes in the potential window spanning from

+1→-3 V (Figure S8 and Table S1, Supporting Information). However, considering our focus from the perspective of proton reduction, redox processes of the monomeric and corresponding fused complex are compared within a potential window ranging from 0→-2V (Figure 1, Table S1, Supporting Information). The cyclic voltammogram of the fused complex **1**, within the aforementioned potential window, reveals three reversible redox features with half wave potentials, $E_{1/2}^{red1} = -0.858$ V, $E_{1/2}^{red2} = -1.156$ V and $E_{1/2}^{red3} = -2.058$ V, against the ferrocene/ferrocenium (FcH/FcH$^+$) redox couple. On the other hand, monomeric complex **2** exhibits, under identical experimental conditions, two reduction processes at half-wave potentials $E_{1/2}^{red1} = -1.655$ V and $E_{1/2}^{red2} = -2.124$ V respectively. The peak separation of (ΔE_p) ~85mV, between the cathodic and anodic waves of all redox processes in both complexes, implies one electron redox processes (considering $\Delta E_p = 80$ mV for the Fc/Fc$^+$ redox couple). It is to be noted that the peak potentials corresponding to the reduction waves of monomeric complex **2** are significantly more negative, with cathodic shifts of 802 and 302 mV, respectively, compared to the first and second reduction processes of dinuclear complex **1**.
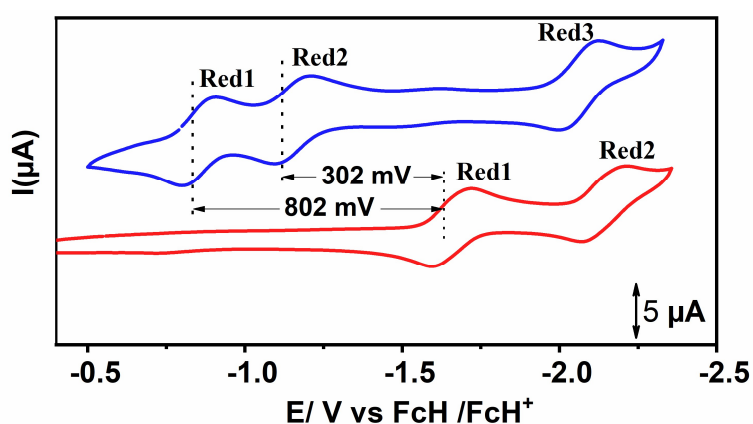
Figure 1. Cyclic voltammograms of triply-fused metalloporphyrin **1** (blue) and monomeric analogue **2** (red) in DMF.

This difference in peak potentials between triply-fused dinuclear metalloporphyrin (**1**) and the monomeric analogue (**2**) in the present investigation, is more pronounced than the difference in redox potentials of the previously reported Cu-complexes of doubly fused and monomeric metalloporphyrins,[27] which is consistent with our motivation for preparing these complexes. Considerable differences in the redox potentials in this case can be realised from the extensive delocalization of electrons across the π-conjugated framework in the triply-fused metalloporphyrin, compared to the monomeric analogue. Furthermore, the corresponding Zn(II)-fused porphyrin displayed identical behaviour under similar experimental conditions, implying a minor influence of the central metal ion on the electrochemical properties of the fused metalloporphyrin, and suggesting ligand-based reductions The electrochemical HOMO-

LUMO gap increases substantially from complex **1** to **2** (1.10 eV and 3.20 eV), in agreement with the observed shift in redox potentials, indicating a greater extent of delocalization in the fused metalloporphyrin compared to the monomer. Moreover, the difference between $E_{1/2}^{ox}$ and $E_{1/2}^{red}$ has been observed to increase significantly from **1** to **2** due to the arrangement of more populated molecular orbitals with increasing conjugation.

Electrochemical data of the complexes have been summarized in Table S1 in the supporting information. Thus, the bimetallic fused porphyrin, with significantly shifted redox potentials in comparison to the monomeric complex, as well as reversibility of the electrochemical processes, encouraged further investigation of these complexes towards electrocatalytic proton reduction.

EPR spectroscopy and Magnetic properties:

To obtain further information regarding the ground state electronic structure of metalloporphyrins **1** and **2**, electron paramagnetic resonance (EPR) analysis has been carried out in combination with magnetic susceptibility measurements (χ *vs* T). EPR spectroscopic measurements of pure solid **1** at 98 K reveal a broad signal containing a multiline pattern due to hyperfine coupling of the electron spin (S = 1) to both ^{63,65}Cu nuclei ($I = 3/2$), as has been observed for Cu(II) dimers reported previously (Figure 2, Table S2, Supporting Information).[29] The best fit to the experimental EPR data was obtained by fitting the spectra obtained from a spin-hamiltonian consisting of an S = 1 spin coupled to two equivalent ^{63,65}Cu(II) nuclei ($I = 3/2$). The good agreement between the simulated and experimental spectra allowed determination of the rhombic **g**-matrix, with *g*-values (g_x, g_y, g_z) of 2.06, 2.00, 2.22. The g_z region shows a partially resolved hyperfine pattern consisting of seven lines with a 1:2:3:4:3:2:1 intensity pattern (with the first five lines clearly resolved), typical of hyperfine interaction with two equivalent ^{63,65}Cu(II) nuclei ($I = 3/2$). The associated A_z-value = 308 MHz is roughly half of the one observed for the monomer, which is indicative of an S = 1 electron spin ($\mathbf{A}_{S=1} = (1/2)\mathbf{A}_{S=1/2}$). [30] The absence of half-field transitions ($\Delta M_s = \pm 2$) even at lower temperature implies weak fine structure interaction, despite the triplet state spin structure, which has also been reported in the literature for diporphyrins with large center to center distances.[31] The hyperfine coupling (hfc) as well as the **g**-matrix components, suggest the spin density is centred on the two Cu(II) centers, with minimal participation of the ligand scaffold, in the ground state. This is supported by density functional calculations (PBE0/def2-TZVP/SVP) that show that the triplet state is appreciably lower in energy than the singlet state ($\Delta E_{S=1 - S=0} \sim$ –2400 cm^{-1}, Figure S11, Supporting Information).
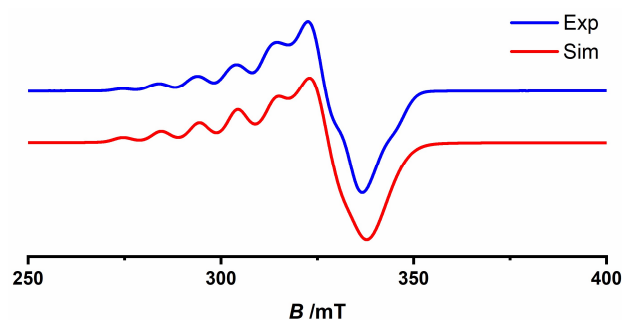
Figure 2. Experimental (blue) and simulated (red) EPR spectra of the complex **1** at 98K.

EPR spectra of mononuclear copper porphyrin (**2**) measured at 98 K display a multiline pattern arising from the hyperfine interaction to a single ^{63,65}Cu ($I = 3/2$) and four ^{14}N (I = 1) nuclei (Figure S10, Supporting Information). The experimental spectrum has been reasonably fitted with by a simulation of an S = 1/2 spin Hamiltonian with hyperfine interaction to the previously described nuclei. The experimental spectrum has been simulated with an axial **g**-matrix with values of $g_{\parallel}$ = 2.19 (A parallel = 596 MHz) and $g_{\perp}$ = 2.045 (A perp = 62 MHz), which agrees well with the data previously reported in the literature.[32]

To further assess the nature of the magnetic interactions between electron spins centered on each Cu(II) of complex **1**, variable temperature magnetic susceptibility (χT) measurements have been carried out, in the temperature range spanning from 0-300 K. At 300 K, an effective magnetic moment value of 0.85 cm^3 mol^{-1} K implies existence of two uncoupled spin doublets (Figure 3). Further, variable temperature measurements disclose temperature independent behavior of the magnetic moment until 40 K, following which a sharp drop in the value has been observed reaching an effective magnetic moment of 0.15 cm^3 mol^{-1} K. This temperature dependent variation of the effective magnetic moment value exhibits resemblance with the
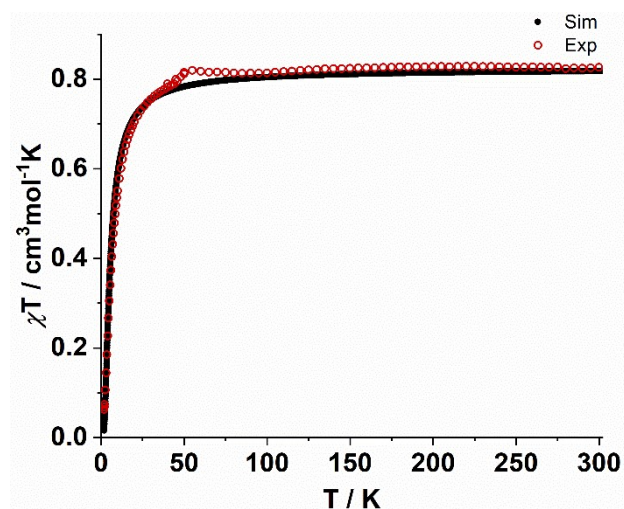

Figure 3. Variable temperature magnetic susceptibility measurements for the complex **1** in the temperature range 0-300 K

Curie-Weiss law, implying a weak antiferromagnetic coupling between the electron spins of the two Cu(II) ions, as has also been previously observed in the case of dinuclear Cu(II) complexes of *meso–meso*, *β– β*, *β – β* triply linked diporphyrin.[33] An exchange coupling constant of J = -6.69 cm^{-1}, obtained via least-squares fitting of the Bleaney-Bowers equation[34] to the susceptibility data, also agrees well with the literature reported data. Further, the value of the magnetic susceptibility (χT) has been found to be consistent with the EPR derived parameters (*g*-values). The small but non-negligible exchange constant, as well as the seven-line hyperfine pattern in the EPR spectrum of **1** underlines the important role of the conjugated bond between individual porphyrin units in the long-range antiferromagnetic coupling.

UV-Vis-NIR Spectroelectrochemistry:

Successive changes in the electronic and vibrational structure of the complexes **1** and **2** upon concomitant reductions have been evaluated via UV-Vis-NIR spectroelectrochemical studies. Spectroelectrochemical measurements provided significant information regarding redox-induced changes in the absorption profile of the monomeric and triply-fused metalloporphyrins, thus allowing comparative analysis of the electronic structure of the two complexes. UV-Vis-NIR absorption profiles of complexes **1** and **2** in DMF reveal significant differences. Consistent with literature reports, complex **1** exhibits three distinct absorption bands, instead of two bands in the case of complex **2** (Figure 4, S12, S13 and Table S3, Supporting Information).[35] along with Q-band transitions centered at 536 nm. Instead, the Soret-like transitions in complex.
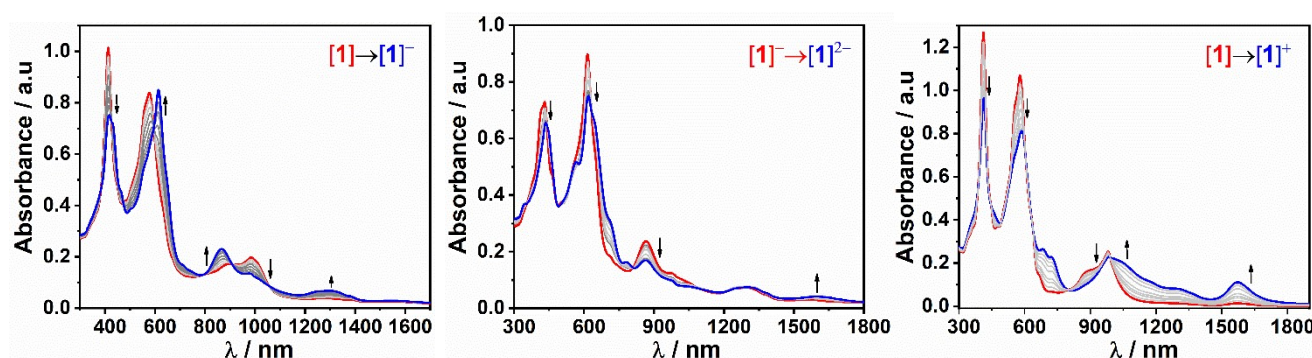
Figure 4. UV-Vis-NIR spectroelectrochemical responses of **1**^{n} in DMF/0.1 M ^{n}Bu$_4$PF$_6$ solution.

Monomeric complex **2** exhibits absorption bands at 417 nm corresponding to Soret transition **1** split into two bands at 414 nm and 576 nm (band I and II), owing to the excitonic coupling between the individual porphyrin units

While the absorption band at 414 nm from **1** occurs at similar energies as for **2**, significant red-shift in the peak position of band II in **1** has been noted. On the other hand, the Q-band like transition in **1** displays significantly red shifted bands at 887 and 986 nm compared to the Q-

bands of **2**; this is attributed to the extensive conjugation between the diporphyrin π-electron systems.

Further, spectroelectrochemical responses of both complexes recorded under identical experimental conditions allow comparative analysis of the absorption spectra of **1** and **2**, upon successive reduction or oxidation processes. In the case of complex **1**, upon reduction, the Soret bands at 414 and 576 nm undergo bathochromic shifts to 415 and 611 nm with distinct isobestic points, inferring stable conversion without an involvement of transient species or decomposition products. On the other hand, the Q-band transitions display hypsochromic shifts to 865 nm in the one electron reduced species 1^- along with an appearance of a new band at 1293 nm which could be attributed to the intra-ligand charge transfer. The monomeric complex **2** exhibits similar behaviour, with an additional band arising at 877 nm in addition to Q-band transition at 666 nm. Further reduction of the monoanionic species leading to the formation of dianionic species 1^{2-}, results in the growth of a low energy NIR band at ~1600 nm with concomitant reduction in intensity of the existing absorption bands. Notably, application of starting potential of 0V to the *in-situ* generated species resulted in the recovery of the UV-Vis spectrum identical to the native species, underlining the reversibility of the redox processes. Spectroelectrochemical response of **1** upon $1e^-$ oxidation results in the decrease in intensity of the Soret bands and blue shift of the Q-bands to 688 and 723 nm, in addition to formation of new low-energy band at 1572 nm, with clearly defined isobestic points, implying formation of porphyrin π-cation radical 1^+. Successive oxidation of the intermediate monocationic species 1^+ to the respective dication exhibits further decrease in intensity of the existing absorption bands.

Electrocatalytic HER studies:

Electrocatalytic activity of the fused and monoporphyrin complexes **1** and **2** towards reduction of protons to hydrogen (HER) has been investigated in DMF with 0.1M $^nBu_4PF_6$ as the supporting electrolyte under Ar in the presence of trifluoroacetic acid (TFA, pK_a = 6.1 in DMF) as a proton source with concentrations ranging from 5mM to 60mM. All the measurements have been performed in a three electrode configuration electrochemical cell equipped with glassy carbon working electrode, Platinum wire as counter electrode and Ag-wire as a pseudoreference with ferrocene/ferrocinium (FcH/FcH^+) redox couple as an internal reference. Electrocatalytic activity of the complex **1** towards HER has been investigated via titration experiments of the 0.01 mM catalyst solution in DMF with varying amounts of TFA. Significantly, upon addition of TFA, a large electrocatalytic current associated with an irreversible cathodic wave appeared at an onset potential of -0.96V, which achieved maximum

current at -1.94 V, with a half-wave potential of -1.42V (Figure 5a and S15, Supporting Information). Notably, appearance of catalytic reduction waves near the $\mathbf{1^{2-}/1^-}$ (second reduction) redox process indicated possible involvement of doubly reduced species in HER. Additionally, justification in favor of the aforementioned observation could be made from the lack of significant changes in the reversible nature of the first reduction wave before and after addition of TFA. Considering the thermodynamic potential required for reduction of TFA in DMF solutions to be ~-0.94 V, the overpotential for HER with the triply-fused metalloporphyrin **1,** was calculated to be ~480 mV taking into account half of the maximum current of its catalytic wave (Figure 5b).

Consistent with the argument provided by Savéant and co-workers[36] regarding ideal CV responses for the catalytic reactions, a typical S-shaped catalytic wave has been recorded at a higher scan rate of 300 mV/s with 15 mM acid concentration (Figure 5b).
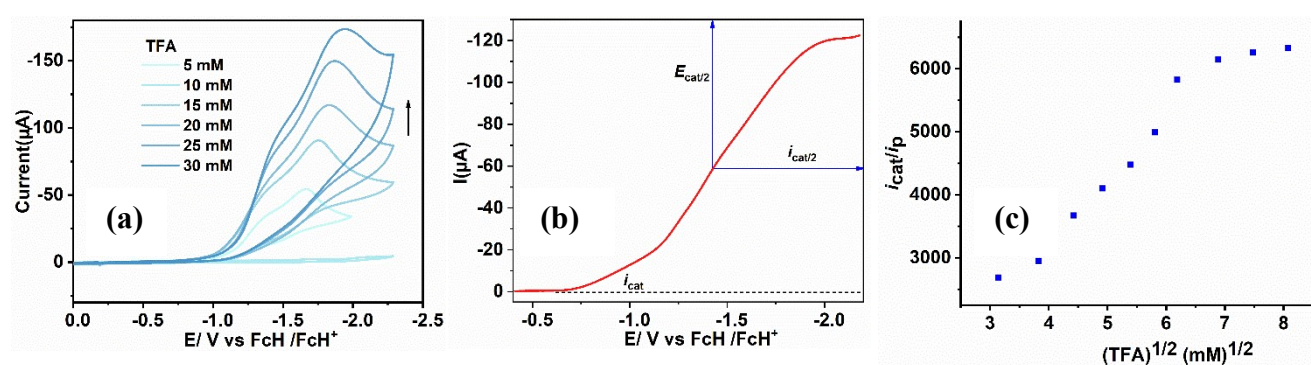

Figure 5. (a) Cyclic voltammetric responses of 0.01 mM DMF solution of **1** with increasing concentration of TFA (Condition: 100 mV/s scan rate, under Ar, 0.1 M $^nBu_4PF_6$). (b) Ideal *S*-shaped cyclic voltammogram of 0.01 mM DMF solution of **1** containing 15 mM of TFA and 0.1 M of electrolyte at 300 mV/s scan rate. (c) Plot of i_{cat}/i_p versus square root of the scan rate.

The electrochemical responses recorded under aforementioned experimental conditions imply that the substrate concentration at the electrode surface is equal to the bulk concentration, referring to the HER activity limited by kinetics of the catalytic reactions instead of diffusion of the substrate protons. Moreover, the linear dependence of peak current (i_p) with the square root of the scan rate ($v^{1/2}$) confirms catalysis in the diffusion-controlled electrochemical regime in this experimental condition (Figure S16, Supporting Information). The catalytic current (i_{cat}) associated with the cathodic wave increases linearly with scan rate following a first-order rate dependence, which in turn highlights the homogeneous nature of the dinuclear Cu-catalyst. Importantly, linear dependence of i_{cat} over scan rate (v) no longer holds when scan rate exceeds 0.5 V/s pointing towards saturation point (Figure S17, Supporting Information). It has also been

observed that the plateau of the catalytic current reaches its maximum when concentrations of TFA are greater than 60 mM; beyond this point, addition of further acid has almost zero effect on the catalytic current (Figure 5c) indicating zeroth-order rate dependence on acid. Notably, complex **2**, under identical experimental conditions (catalyst concentration of 0.01 mM and acid concentration of 15 mM) displays irreversible cathodic waves with a significant cathodic shift (~600 mV) in the onset potential of electrochemical HER, compared to that of complex **1**, underlining higher activity of the complex **2** over complex **1** (Figure 6). Moreover, comparison of the catalytic efficiency with the same concentrations of catalysts (0.01 mM) and acid (15 mM) indicate that complex **2** produces equivalent amounts of current at much higher overpotential (~800 mV) with respect to **1**. Thus, catalyst **1** lowers the overpotential by ~320 mV compared to **2** for catalytic proton reduction, indicating the enhanced activity of the former complex.

Since **1** possesses two individual Cu(II)-containing porphyrin centers fused together, evaluation of the electrochemical HER activity has also been performed using twice as much concentration (0.02 mM) of **2** against 0.01 mM of **1** with a fixed acid concentration (15 mM). Moreover, comparison of potentials for HER with the higher concentration (0.02 mM) of complex **2** with respect to 0.01 mM solution of complex **1** has also been performed.
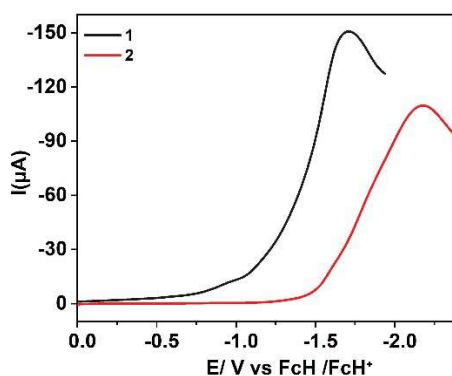
Figure 6. Linear sweep voltammograms of 0.01 mM DMF solutions of **1** (black) and **2** (red) with 0.1 M $^{n}Bu_4PF_6$ in the presence of 15 mM of TFA at 100 mV/s.

. Linear sweep voltammograms of 0.01 and 0.02 mM solutions of **1** and **2**, respectively, under otherwise identical experimental conditions, reveal that higher concentration solution of complex **2** exhibit catalytic activity at potentials ~300 mV negative to that of the lower concentration solution of complex **1**(Figure S18, Supporting Information). This observation clearly suggests better catalytic efficiency of **1** over **2** towards catalytic HER. Importantly, addition of 15mM of TFA to a DMF solution containing 0.1 M $^{n}Bu_4PF_6$ in the absence of catalyst showed no catalytic currents under otherwise similar experimental conditions (scan

rate: 100 mV/s) (Figure S19, Supporting Information). On the other hand, electrochemical measurements containing 0.01 mM solution of the Zn-complexes of triply-fused porphyrin **3** in presence of TFA (15 mM) under identical experimental conditions (0.1 M $^nBu_4PF_6$, scan rate: 100 mV/s) displayed a ~400 mV cathodically shifted onset potential compared to **1**, highlighting the remarkable activity of the Cu-containing complex **1** (Figure S19, Supporting Information).

Following the performance of the catalyst in HER, we have performed different control experiments to rule out possible effects of various components in the catalytic processes. Initially, to exclude the role of catalyst deposition on the electrode surface during the course of electrocatalytic process, the glassy carbon electrode utilized in the catalytic proton reduction reaction was taken out of the solution and rinsed properly to get rid of the physisorbed species and dipped into a solution of DMF containing only 15 mM of TFA and 0.1 M of $^nBu_4PF_6$ in the absence of a catalyst. Electrochemical measurements performed under this setup revealed absence of any catalytic current above the background, negating any adsorption of the active catalysts onto the electrode surface (Figure S20, Supporting Information). Moreover, electrochemical experiments with Hg-pool working electrode were conducted to detect involvement of metal nanoparticles in proton reduction, since metal nanoparticles are sometimes inactivated in the presence of Hg(0) due to adsorption or amalgamation. However, the measured current with the Hg-pool electrode exhibits no significant difference to that of the electrocatalytic measurements carried out with the GC electrode. Since no loss in catalytic activity was detected in the presence of Hg-pool electrode, the observation was consistent with the notion that metal-nanoparticles were not responsible for catalytic activity, underlining role of molecular catalyst **1** in the HER (Figure S21, Supporting Information).[37] Further, control experiments using a glassy carbon counter electrode in place of platinum wire, revealed no such noticeable differences in the electrochemical behavior of the catalysts, eliminating a possible role of leached platinum particles in the electrocatalytic process (Figure S22, Supporting Information). [38] Additionally, stability of **1** in acidic solution during the course of electrocatalytic HER has been evaluated through UV-Vis-NIR spectroscopic monitoring. Analysis of the absorption spectra of the catalyst in a 1:1 (v/v) mixture of TFA and DMF revealed no change in the spectra even after keeping the solution for a prolonged time in the dark. This indicates that the tetrapyrrolic core of the catalyst remains intact with no sign of demetallated species as confirmed from ESI-MS analysis of the solution (Figure S23, Supporting Information).

After establishing the role of the molecular catalyst towards proton reduction, we calculated the catalytic rate constant (k_{obs}), also referred to as turnover frequency, to compare the efficiency of the catalysts utilized in this study with previously reported systems. The observed rate constant (k_{obs}) was calculated from the ratio of catalytic current (i_{cat}) and peak current (i_p) following equation S3 (Figure 5c, S24 and Table S4, Supporting Information) at each concentrations of acid solution and a scan rate of 300 mV/s.[36,39] The rate constant calculated via this method was found to be 0.5 x 10^7 s^{-1}(conc. of TFA: 15 mM), which is significantly higher than that of the previously reported doubly fused dinuclear copper complex.[27] As discussed previously, when catalytic current (i_{cat}) no longer increases beyond a scan rate of 0.6 V/s and holds proportional relationship with square root of the concentration of TFA, rate constant (k_{obs}) becomes directly proportional to TFA concentration (equation S3, Supporting Information). Under this condition, k_{obs} becomes first order with respect to acid concentration (Figure S24, Supporting Information). However, k_{obs} follows a zeroth order dependence with respect to the acid concentration, under the condition when catalytic current (i_{cat}) no longer exhibits any significant changes upon addition of acid (~60 mM). Although direct comparison among HER catalysts is quite difficult given the complexity and diversity associated with various experimental conditions, the reported rate constant for **1** is remarkably high, amongst the highest reported in the literature.

To quantify the amount of hydrogen evolved during the process of catalytic HER, controlled potential electrolysis of **1** and **2** has been carried out in a gas-tight H-type cell separated by a microporous membrane. Linear Sweep Voltammetric (LSV) experiments, carried out with 0.06 and 0.12 mM DMF solutions of complexes **1** and **2**, revealed better efficiency of the catalyst **1** in comparison to the **2**, ascertained from the lower onset potential and nearly 4-fold increase in the current density of the former against the latter (Figure 7).
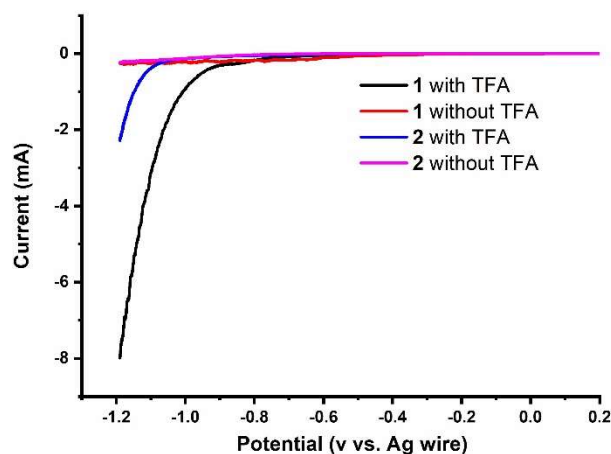
Figure 7. Linear Sweep Voltammograms of 0.06mM and 0.12mM DMF solutions of bimetallic fused (**1**) and monomeric (**2**) copper porphyrin.

Bulk electrolysis measurements have been performed with a 0.06 mM and 0.12 mM solution of **1** or **2**, respectively, in 30 mL DMF solution containing 0.1 M TFA, at a potential of -1.05 V, under N_2 atmosphere. During the electrolysis process, constant cathode potential was maintained and the amount of H_2 formed was detected via gas chromatographic analysis (Figure S25, Supporting Information). Faradaic efficiency of complexes **1** and **2** upon controlled potential electrolysis conducted for 30 minutes, has been calculated to be 96.6% and 71.2% respectively, underlining enhanced catalytic performance of the dinuclear framework as compared to the mononuclear one towards electrochemical HER (Figure 8). Turnover number for both **1** and **2** has been calculated to be 102 and 18.39 (Figure 8), which indeed supports increased catalytic activity/stability of the bimetallic copper porphyrin against the respective copper porphyrin monomer. After each bulk electrolysis measurement, the carbon paper working electrode was removed from the electrolyte, rinsed three times with DMF, and reinstalled again to perform blind experiments. Therefore, linear sweep voltammograms were recorded with a fresh solution of DMF containing 0.1 M $^nBu_4PF_6$ and 0.1 M TFA, without any catalysts. Lack of any substantial background current as compared to the current density obtained with the catalyst **1** and **2** rules out any involvement of adsorbed catalytic species such as Cu nanoparticles deposited onto the electrode surface during the electrocatalytic process (Figure S26 and S27, Supporting Information). Further, absorption studies of the catalyst before and after electrolysis exhibit no significant changes in the spectrum (Figure S28, Supporting Information), which verifies the stability of the catalyst during the course of electrocatalytic H_2 evolution.
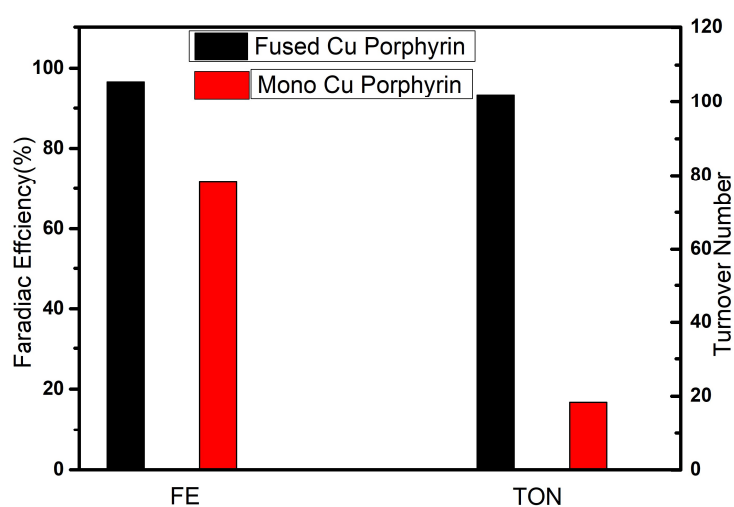
Figure 8. Comparison of Faradaic Efficiency and Turnover number between complex **1** and **2**.

Further, RRDE experiment has been performed with 0.01 mM solution of complex **1** containing 0.1 M of electrolyte in presence of 3 mM of TFA at rotation rates between 500 to 2000 RPM.

Potential of the platinum ring electrode was held at a constant potential of 1.23 V while potentials of glassy carbon disk electrode was swept at a 100 mV/s scan rate towards negative potentials (Figure S29 and S30, Supporting Information). Under the experimental condition mentioned above corresponding ring and disk current has been recorded and the ratio of these two in combination with collection efficiency was utilized to determine the faradaic efficiency (Figure S29 and S30, Supporting Information). Notably, collection efficiency, determined with 10 mM potassium ferricyanide in aqueous electrolyte solution of 1M potassium nitrate, has been calculated to be 22.9%. The faradaic efficiency for the 0.01 mM solution of complex **1** and **2** using equation S4 (Supporting Information)[40] has been calculated to be 88(±6)% and 44(±8)% (Equation S4 and Figure S29-S30, Supporting Information) respectively.

To understand the role of probable intermediate species in the proton reduction process, one- and two-electron reduced species of the complex **1** were generated both electrochemically as well as through chemical reduction. Further, reaction of these *in situ* generated species with TFA was also studied via spectroelectrochemical techniques to get insights into the HER mechanism. Dinuclear complex **1** was first treated with a stoichiometric amount of cobaltocene (CoCp$_2$) in CH$_2$Cl$_2$, resulting in the formation of light green colored one-electron reduced species **1$^-$**, as ascertained from the UV-Vis-NIR spectroscopic studies. Notably, absorption spectra of chemically generated **1$^-$** species was observed to be well in agreement with the electrochemically generated one-electron reduced species (Figure S31 and S32, Supporting Information) with clearly defined isosbestic points suggesting complete conversion. Addition of TFA to **1$^-$**, leads to a new UV-Vis spectrum with simultaneous change in color of the solution from light green to yellow (Figure S31 and S32, Supporting Information). Moreover, addition of large excess of TFA to this solution did not induce any significant spectral changes, which implies lack of basicity of this one electron reduced species to drive the protonolysis further. Thus, further reduction of **1$^-$** is necessary to facilitate the catalytic phenomenon. To generate the doubly reduced species **1^{2-}**, excess of NaBH$_4$/KC$_8$ was added into the DMF solution of **1**, resulting in an immediate change in color of the solution from violet to deep green, indicating formation of the desired doubly reduced species as confirmed from the changes in the absorption spectra (Figure 9a). Similarity in the absorption spectrum of **1^{2-}** generated either electrochemically or chemically, along with well-defined isobestic points confirms complete conversion of the ground state species to the doubly reduced form (Figure 9b). Importantly, treatment of the doubly reduced species with excess amount of TFA gave altered absorption spectra, which after some time slowly decays back to regenerate the initial species **1**, as confirmed from the identical UV-Vis-NIR spectrum of the reduced species containing TFA

with that of the initial form (Figure 9c). Conversion of the two electron reduced species to the initial species can also be followed from the noticeable change in color of the
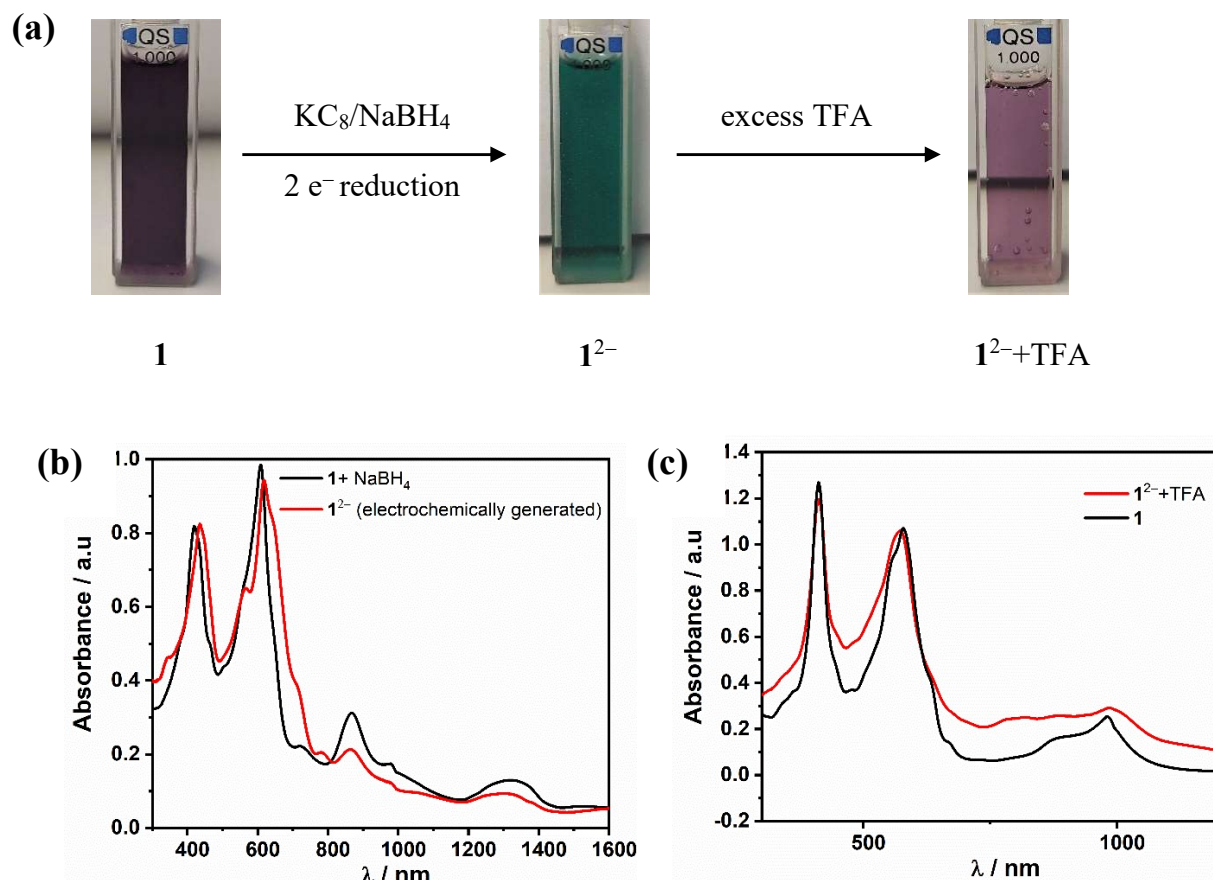

Figure 9. (a) Change in colour of the DMF solution of **1** upon two electron reduction (deep green) and reaction of the reduced species with TFA to regenerate the native species, (b)UV-Vis-NIR absorption spectra of the electrochemically (red) and chemically (black) generated doubly reduced species, and (c) Absorption spectra of the reaction of doubly reduced species with excess TFA (red) and native species **1** (black), and (c)

solution from deep green to violet (Figure 9a). Further, EPR spectroscopic analyses of the one- and two-electron reduced species and their reaction with TFA displayed similar behaviour to the UV-Vis-NIR studies, wherein doubly reduced species **1**$^{2-}$, generated via chemical reduction, on treatment with excess of TFA, reverts to the initial species **1**, as observed from the identical EPR spectra (Figure 10). Similarity in the absorption spectra obtained from electrochemical and chemical reduction emphasises identical redox behaviours of the transient species under chemical and electrochemical treatment. Thus, the aforementioned experimental observations strongly suggest possible involvement of the doubly reduced form, **1**$^{2-}$ as a catalytically active species towards electrochemical reduction of protons to hydrogen.

On the basis of information obtained from experimental analysis, it could be predicted that ground state species **1** undergoes two electron reduction to form doubly reduced species **1**$^{2-}$,

which subsequently reacts with protons generating a probable hydride intermediate. The intermediate species so formed, in presence of excess amount of TFA, reacts with a second proton to generate initial species along with the release of hydrogen. However, presence of two
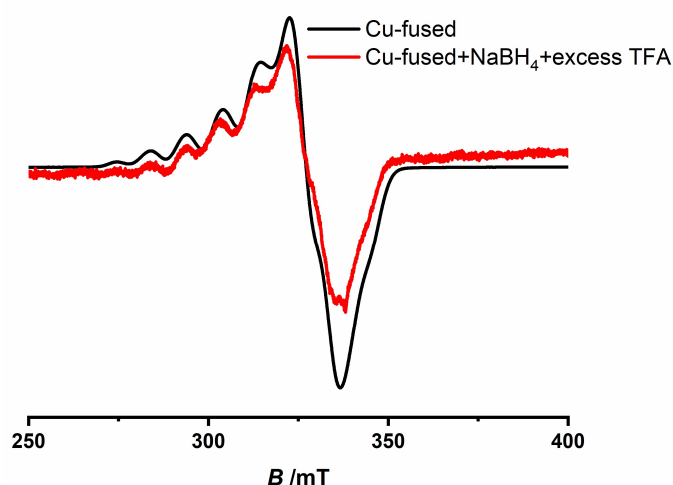
Figure 10. EPR spectra of the reaction of doubly reduced species (1^{2-}) with excess TFA (red) and native species **1** (black).

metals in the conjugated porphyrin system allows for a competitive scenario involving formation of a bimetallic hydride species. The extremely fast turnover frequency of **1** towards H_2 evolution implies very reactive intermediates which at this point haven't been isolated or detected spectroscopically. Future mechanistic studies on this promising system will help elucidate the details of the catalytic cycle and hopefully provide insights into the structure-function relationships of bimetallic Cu triply-fused porphyrins as H_2 evolution catalysts.

Conclusion:

In summary, bimetallic copper complex (**1**) featuring a triply-fused porphyrin framework and respective non-fused monomeric complex have been synthesized to draw a correlation between their catalytic properties towards electrocatalytic proton reduction. As indicated by cyclic voltammetric analysis, reduction processes in case of fused porphyrin complex occurs at lower applied bias potential, compared to the nonfused complex, with a difference of ~800 mV between the first reduction processes of each complex. Such a large margin of difference in reduction potentials could be attributed to the extended delocalization of electrons within the fused porphyrin framework, allowing easy tunability of the redox properties as compared to the well-known methods of using electron deficient functional groups to fine-tune the electrochemical potential in energy driven processes. Notably, the bimetallic complex **1** exhibit increased activity and lower onset potential towards proton reduction, compared to the mononuclear complex **2**. Consistent with the enhanced electrocatalytic activity, the fused

dicopper porphyrin complex significantly reduces the overpotential (by ~ 320 mV), compared to the mononuclear copper porphyrin, required to generate equivalent amounts of current. These results taken together suggest positive impact of the fused scaffold over monomeric porphyrins on proton reduction, which is also reflected by the significantly higher faradaic efficiency of the dinuclear complex (Faradaic efficiency: 97% for **1** and 71% for **2**). Further, the observed rate constant (k_{obs}) of 0.5×10^7 s^{-1} (conc. of TFA: 15 mM), calculated from the kinetic analysis, is one of the highest reported rate constants so far. Although, further analysis regarding identification of the mechanistic pathway as well as probable intermediates is necessary, we could already show here that the two-electron reduced metal complex is likely the active catalyst for the electrochemical HER. To the best of our knowledge, this is the first time a metal complex (any metal) of a triply fused biporphyrin ligand has been used as a molecular electrocatalyst. Considering the excellent catalytic parameters obtained in this investigation (low over potential, stability of the molecular catalyst, high turnover numbers, and high rate constants), we expect metal complexes of triply fused biporphyrin ligands to play a very important role in energy related electrocatalytic work in the future.

Supporting Information:

Supporting information for this article containing following details is available;
Experimental section, NMR spectra, Cyclic voltammetry, Spectroelectrochemical measurements, electrocatalytic studies, and DFT.

Refernces:

[1] a) R. Cao, W. Lai, P. Du, *Energy Environ. Sci.* **2012**, *5*, 8134; b) T. R. Cook, D. K. Dogutan, S. Y. Reece, Y. Surendranath, T. S. Teets, D. G. Nocera, *Chemical reviews* **2010**, *110*, 6474; c) M. Grätzel, *Nature* **2001**, *414*, 338; d) H. B. Gray, *Nature chemistry* **2009**, *1*, 7; e) D. G. Nocera, *Accounts of chemical research* **2012**, *45*, 767; f) Y. Wu, M. Chen, Y. Han, H. Luo, X. Su, M.-T. Zhang, X. Lin, J. Sun, L. Wang, L. Deng et al., *Angewandte Chemie (International ed. in English)* **2015**, *54*, 4870.

[2] a) E. S. Andreiadis, P.-A. Jacques, P. D. Tran, A. Leyris, M. Chavarot-Kerlidou, B. Jousselme, M. Matheron, J. Pécaut, S. Palacin, M. Fontecave et al., *Nature chemistry* **2013**, *5*, 48; b) Z. Han, F. Qiu, R. Eisenberg, P. L. Holland, T. D. Krauss, *Science (New York, N.Y.)* **2012**, *338*, 1321; c) A. Le Goff, V. Artero, B. Jousselme, P. D. Tran, N. Guillet, R. Métayé, A. Fihri, S. Palacin, M. Fontecave, *Science (New York, N.Y.)* **2009**, *326*, 1384; d) A. Onoda, Y. Kihara, K. Fukumoto, Y. Sano, T. Hayashi, *ACS Catal.* **2014**, *4*, 2645; e) F. Wang, W.-G. Wang, H.-Y. Wang, G. Si, C.-H. Tung, L.-Z. Wu, *ACS Catal.* **2012**, *2*, 407.

[3] J. L. Dempsey, B. S. Brunschwig, J. R. Winkler, H. B. Gray, *Accounts of chemical research* **2009**, *42*, 1995.

[4] a) S. Dey, A. Rana, S. G. Dey, A. Dey, *ACS Catal.* **2013**, *3*, 429; b) B. H. Solis, A. G. Maher, T. Honda, D. C. Powers, D. G. Nocera, S. Hammes-Schiffer, *ACS Catal.* **2014**, *4*, 4516.

[5] M. L. Helm, M. P. Stewart, R. M. Bullock, M. R. DuBois, D. L. DuBois, *Science (New York, N.Y.)* **2011**, *333*, 863.

[6] a) I. Roger, M. A. Shipman, M. D. Symes, *Nat Rev Chem* **2017**, *1*; b) A. Barrozo, M. Orio, *ChemSusChem* **2019**, *12*, 4905; c) S. Fukuzumi, Y.-M. Lee, W. Nam, *Coordination Chemistry Reviews* **2018**, *355*, 54.

[7] M. A. Abbas, J. H. Bang, *Chem. Mater.* **2015**, *27*, 7218.

[8] a) M. E. Carroll, B. E. Barton, T. B. Rauchfuss, P. J. Carroll, *Journal of the American Chemical Society* **2012**, *134*, 18843; b) S. Kaur-Ghumaan, L. Schwartz, R. Lomoth, M. Stein, S. Ott, *Angewandte Chemie (International ed. in English)* **2010**, *49*, 8033; c) M. J. Rose, H. B. Gray, J. R. Winkler, *Journal of the American Chemical Society* **2012**, *134*, 8310.

[9] a) B. Mondal, K. Sengupta, A. Rana, A. Mahammed, M. Botoshansky, S. G. Dey, Z. Gross, A. Dey, *Inorganic chemistry* **2013**, *52*, 3381; b) O. Pantani, S. Naskar, R. Guillot, P. Millet, E. Anxolabéhère-Mallart, A. Aukauloo, *Angewandte Chemie (International ed. in English)* **2008**, *47*, 9948; c) W. M. Singh, T. Baine, S. Kudo, S. Tian, X. A. N. Ma, H. Zhou, N. J.

DeYonker, T. C. Pham, J. C. Bollinger, D. L. Baker et al., *Angewandte Chemie (International ed. in English)* **2012**, *51*, 5941; d) Y. Sun, J. P. Bigi, N. A. Piro, M. L. Tang, J. R. Long, C. J. Chang, *Journal of the American Chemical Society* **2011**, *133*, 9212.

[10]   a) R. Bar-Ziv, P. Ranjan, A. Lavie, A. Jain, S. Garai, A. Bar Hen, R. Popovitz-Biro, R. Tenne, R. Arenal, A. Ramasubramaniam et al., *ACS Appl. Energy Mater.* **2019**, *2*, 6043; b) H. I. Karunadasa, C. J. Chang, J. R. Long, *Nature* **2010**, *464*, 1329; c) H. I. Karunadasa, E. Montalvo, Y. Sun, M. Majda, J. R. Long, C. J. Chang, *Science (New York, N.Y.)* **2012**, *335*, 698; d) H. Vrubel, D. Merki, X. Hu, *Energy Environ. Sci.* **2012**, *5*, 6136.

[11]   a) A. M. Abudayyeh, O. Schott, H. L. C. Feltham, G. S. Hanan, S. Brooker, *Inorg. Chem. Front.* **2021**, *8*, 1015; b) M. Kügler, J. Scholz, A. Kronz, I. Siewert, *Dalton transactions (Cambridge, England : 2003)* **2016**, *45*, 6974; c) X. Liu, S. Cui, Z. Sun, P. Du, *Chemical communications (Cambridge, England)* **2015**, *51*, 12954.

[12]   a) M. Gong, D.-Y. Wang, C.-C. Chen, B.-J. Hwang, H. Dai, *Nano Res.* **2016**, *9*, 28; b) A. M. Appel, D. H. Pool, M. O'Hagan, W. J. Shaw, J. Y. Yang, M. Rakowski DuBois, D. L. DuBois, R. M. Bullock, *ACS Catal.* **2011**, *1*, 777; c) O. R. Luca, S. J. Konezny, J. D. Blakemore, D. M. Colosi, S. Saha, G. W. Brudvig, V. S. Batista, R. H. Crabtree, *New J. Chem.* **2012**, *36*, 1149; d) U. J. Kilgore, J. A. S. Roberts, D. H. Pool, A. M. Appel, M. P. Stewart, M. R. DuBois, W. G. Dougherty, W. S. Kassel, R. M. Bullock, D. L. DuBois, *Journal of the American Chemical Society* **2011**, *133*, 5861.

[13]   W. A. Hoffert, J. A. S. Roberts, R. Morris Bullock, M. L. Helm, *Chemical communications (Cambridge, England)* **2013**, *49*, 7767.

[14]   a) F. A. Armstrong, J. Hirst, *Proceedings of the National Academy of Sciences of the United States of America* **2011**, *108*, 14049; b) M. Rakowski DuBois, D. L. DuBois, *Chemical Society reviews* **2009**, *38*, 62; c) M. Sadakane, E. Steckhan, *Chemical reviews* **1998**, *98*, 219.

[15]   J. R. McKone, S. C. Marinescu, B. S. Brunschwig, J. R. Winkler, H. B. Gray, *Chem. Sci.* **2014**, *5*, 865.

[16]   W. Lubitz, H. Ogata, O. Rüdiger, E. Reijerse, *Chemical reviews* **2014**, *114*, 4081.

[17]   H. S. Shafaat, O. Rüdiger, H. Ogata, W. Lubitz, *Biochimica et biophysica acta* **2013**, *1827*, 986.

[18]   a) K. Hou, H. T. Poh, W. Y. Fan, *Chemical communications (Cambridge, England)* **2014**, *50*, 6630; b) T. Fang, H.-X. Lu, J.-X. Zhao, S.-Z. Zhan, Q.-Y. Lv, *Journal of Molecular Catalysis A: Chemical* **2015**, *396*, 304; c) J.-P. Cao, T. Fang, Z.-Q. Wang, Y.-W. Ren, S. Zhan, *Journal of Molecular Catalysis A: Chemical* **2014**, *391*, 191; d) E. A.

Mohamed, Z. N. Zahran, Y. Naruta, *Chemical communications (Cambridge, England)* **2015**, *51*, 16900.

[19]   a) W. Auwärter, D. Écija, F. Klappenberger, J. V. Barth, *Nature chemistry* **2015**, *7*, 105; b) W. M. Campbell, K. W. Jolley, P. Wagner, K. Wagner, P. J. Walsh, K. C. Gordon, L. Schmidt-Mende, M. K. Nazeeruddin, Q. Wang, M. Grätzel et al., *J. Phys. Chem. C* **2007**, *111*, 11760; c) J. S. Lindsey, D. F. Bocian, *Accounts of chemical research* **2011**, *44*, 638; d) N. K. Subbaiyan, C. A. Wijesinghe, F. D'Souza, *Journal of the American Chemical Society* **2009**, *131*, 14646; e) J. R. Swierk, D. D. Méndez-Hernández, N. S. McCool, P. Liddell, Y. Terazono, I. Pahk, J. J. Tomlin, N. V. Oster, T. A. Moore, A. L. Moore et al., *Proceedings of the National Academy of Sciences of the United States of America* **2015**, *112*, 1681.

[20]   a) I. Bhugun, D. Lexa, J.-M. Savéant, *J. Am. Chem. Soc.* **1996**, *118*, 3982; b) C. Costentin, S. Drouet, M. Robert, J.-M. Savéant, *Science (New York, N.Y.)* **2012**, *338*, 90; c) C. Costentin, M. Robert, J.-M. Savéant, *Chemical Society reviews* **2013**, *42*, 2423; d) C. Costentin, M. Robert, J.-M. Savéant, *Accounts of chemical research* **2015**, *48*, 2996; e) T. Dhanasekaran, J. Grodkowski, P. Neta, P. Hambright, E. Fujita, *J. Phys. Chem. A* **1999**, *103*, 7742; f) S. Lin, C. S. Diercks, Y.-B. Zhang, N. Kornienko, E. M. Nichols, Y. Zhao, A. R. Paris, D. Kim, P. Yang, O. M. Yaghi et al., *Science (New York, N.Y.)* **2015**, *349*, 1208; g) S. Losse, J. G. Vos, S. Rau, *Coordination Chemistry Reviews* **2010**, *254*, 2492; h) A. Maurin, M. Robert, *Journal of the American Chemical Society* **2016**, *138*, 2492.

[21]   a) B. B. Beyene, C.-H. Hung, *Coordination Chemistry Reviews* **2020**, *410*, 213234; b) C.-M. Che, V. K.-Y. Lo, C.-Y. Zhou, J.-S. Huang, *Chemical Society reviews* **2011**, *40*, 1950; c) X. Guo, N. Wang, X. Li, Z. Zhang, J. Zhao, W. Ren, S. Ding, G. Xu, J. Li, U.-P. Apfel et al., *Angewandte Chemie (International ed. in English)* **2020**, *59*, 8941; d) G. F. Moore, J. D. Blakemore, R. L. Milot, J. F. Hull, H.-e. Song, L. Cai, C. A. Schmuttenmaer, R. H. Crabtree, G. W. Brudvig, *Energy Environ. Sci.* **2011**, *4*, 2389; e) L. Xie, J. Tian, Y. Ouyang, X. Guo, W. Zhang, U.-P. Apfel, W. Zhang, R. Cao, *Angewandte Chemie (International ed. in English)* **2020**, *59*, 15844; f) G. Xu, H. Lei, G. Zhou, C. Zhang, L. Xie, W. Zhang, R. Cao, *Chemical communications (Cambridge, England)* **2019**, *55*, 12647; g) W. Zhang, W. Lai, R. Cao, *Chemical reviews* **2017**, *117*, 3717.

[22]   D. K. Bediako, B. H. Solis, D. K. Dogutan, M. M. Roubelakis, A. G. Maher, C. H. Lee, M. B. Chambers, S. Hammes-Schiffer, D. G. Nocera, *Proceedings of the National Academy of Sciences of the United States of America* **2014**, *111*, 15001.

[23]   a) D. J. Graham, D. G. Nocera, *Organometallics* **2014**, *33*, 4994; b) B. H. Solis, A. G. Maher, D. K. Dogutan, D. G. Nocera, S. Hammes-Schiffer, *Proceedings of the National Academy of Sciences of the United States of America* **2016**, *113*, 485.

[24]   a) C. W. Li, J. Ciston, M. W. Kanan, *Nature* **2014**, *508*, 504; b) C. W. Li, M. W. Kanan, *J. Am. Chem. Soc.* **2012**, *134*, 7231; c) A. Paracchino, N. Mathews, T. Hisatomi, M. Stefik, S. D. Tilley, M. Grätzel, *Energy Environ. Sci.* **2012**, *5*, 8673; d) P. D. Tran, M. Nguyen, S. S. Pramana, A. Bhattacharjee, S. Y. Chiam, J. Fize, M. J. Field, V. Artero, L. H. Wong, J. Loo et al., *Energy Environ. Sci.* **2012**, *5*, 8912; e) K. Maeda, T. Ohno, K. Domen, *Chem. Sci.* **2011**, *2*, 1362.

[25]   a) H. Lei, H. Fang, Y. Han, W. Lai, X. Fu, R. Cao, *ACS Catal.* **2015**, *5*, 5145; b) K. Sudhakar, A. Mahammed, Q.-C. Chen, N. Fridman, B. Tumanskii, Z. Gross, *ACS Appl. Energy Mater.* **2020**, *3*, 2828.

[26]   a) A. Tsuda, H. Furuta, A. Osuka, *J. Am. Chem. Soc.* **2001**, *123*, 10304; b) A. Tsuda, A. Osuka, *Science (New York, N.Y.)* **2001**, *293*, 79; c) Y. Inokuma, N. Ono, H. Uno, D. Y. Kim, S. B. Noh, D. Kim, A. Osuka, *Chemical communications (Cambridge, England)* **2005**, 3782; d) S. Hiroto, A. Osuka, *The Journal of organic chemistry* **2005**, *70*, 4054.

[27]   D. Khusnutdinova, B. L. Wadsworth, M. Flores, A. M. Beiler, E. A. Reyes Cruz, Y. Zenkov, G. F. Moore, *ACS Catal.* **2018**, *8*, 9888.

[28]   J. Jökel, F. Schwer, M. von Delius, U.-P. Apfel, *Chem. Commun.* **2020**, *56*, 14179.

[29]   M. Mares-Guia, E. Shaw, *Journal of Biological Chemistry* **1965**, *240*, 1579.

[30]   a) E. I. Solomon, D. E. Heppner, E. M. Johnston, J. W. Ginsbach, J. Cirera, M. Qayyum, M. T. Kieber-Emmons, C. H. Kjaergaard, R. G. Hadt, L. Tian, *Chemical reviews* **2014**, *114*, 3659; b) N. I. Neuman, E. Burna, R. Baggio, M. C. G. Passeggi, A. C. Rizzi, C. D. Brondino, *Inorg. Chem. Front.* **2015**, *2*, 837.

[31]   a) T. M. Bräuer, Q. Zhang, K. Tiefenbacher, *J. Am. Chem. Soc.* **2017**, *139*, 17500; b) N. TOYAMA, M. ASANO-SOMEDA, Y. KAIZU, *Molecular Physics* **2003**, *101*, 733.

[32]   a) J. M. Assour, *The Journal of Chemical Physics* **1965**, *43*, 2477; b) Y. Hsu, *Molecular Physics* **1971**, *21*, 1087.

[33]   T. Ikeue, K. Furukawa, H. Hata, N. Aratani, H. Shinokubo, T. Kato, A. Osuka, *Angewandte Chemie (International ed. in English)* **2005**, *44*, 6899.

[34]   B. Bleaney, K. D. Bowers, *Proc. R. Soc. Lond. A* **1952**, *214*, 451.

[35]   A. A. Ryan, M. O. Senge, *Eur. J. Org. Chem.* **2013**, *2013*, 3700.

[36]   V. Artero, J.-M. Saveant, *Energy Environ. Sci.* **2014**, *7*, 3808.

[37]   a) R. H. Crabtree, *Chemical reviews* **2012**, *112*, 1536; b) J. A. Widegren, R. G. Finke, *Journal of Molecular Catalysis A: Chemical* **2003**, *198*, 317; c) V. Artero, M. Fontecave, *Chemical Society reviews* **2013**, *42*, 2338; d) K. J. Lee, B. D. McCarthy, J. L. Dempsey, *Chemical Society reviews* **2019**, *48*, 2927.

[38]   J. G. Chen, C. W. Jones, S. Linic, V. R. Stamenkovic, *ACS Catal.* **2017**, *7*, 6392.

[39]   a) C. Costentin, J.-M. Savéant, *CHEMELECTROCHEM* **2014**, *1*, 1226; b) K. J. Lee, N. Elgrishi, B. Kandemir, J. L. Dempsey, *Nat Rev Chem* **2017**, *1*; c) E. S. Rountree, B. D. McCarthy, T. T. Eisenhart, J. L. Dempsey, *Inorganic chemistry* **2014**, *53*, 9983.

[40]   a) C. C. L. McCrory, S. Jung, J. C. Peters, T. F. Jaramillo, *J. Am. Chem. Soc.* **2013**, *135*, 16977; b) T. Naresh Kumar, S. Sivabalan, N. Chandrasekaran, K. L. Phani, *Chem. Commun.* **2015**, *51*, 1922; c) D. K. Bediako, Y. Surendranath, D. G. Nocera, *J. Am. Chem. Soc.* **2013**, *135*, 3662.

Table of Contents

Bimetallic triply fused copper containing metalloporphyrin (**1**) is shown to display enhanced activity towards electrochemical proton reduction over its monomeric counterpart (**2**)

- $k_{obs} \sim 10^7\,\text{s}^{-1}$
- *overpotential 1<<2*